A wideband microstrip antenna employing ring and hexadecagonal slots with parasitic elements for W-band applications

AbdulGuddoos S. A. Gaid[1], Mohammed M. S. Qaid[1], Mohammed A. E. Abdullah[1], Mohammad Ahmed Alomari[2]

[1]Department of Communications and Computer Engineering, Faculty of Engineering and Information Technology, Taiz University, Taiz, Yemen
[2]Department of Engineering Technology, Faculty of Technology and Electronic and Computer Engineering (FTKEK), Universiti Teknikal Malaysia Melaka (UTeM), Melaka, Malaysia

Article Info

ABSTRACT

This article presents a monopole patch antenna, designed for operation in the W-band. The antenna is constructed on Rogers/RT 5880 dielectric material with dimensions of 3.4×4×0.16 mm³, a loss tangent of 0.0009, and a relative permittivity of 2.2. The initial design features a simple rectangular patch measuring 1.3542×1.0306 mm², powered by a microstrip line using an inset feed. To enhance the bandwidth and gain, two parasitic rectangular elements were added on both sides of the patch in addition to the incorporation of a circular ring slot with the ground plane. Further improvements in bandwidth and return loss were achieved by etching a hexadecagonal-shaped slot on the patch. Simulation results indicate that the optimized design achieves an impedance bandwidth of 28.54 GHz, ranging from 79.67 GHz to 108.21 GHz, centered at 88 GHz. The antenna also shows a maximum return loss of 59 dB and a voltage standing wave ratio (VSWR) of 1.0022. The radiation pattern is directional, with a peak gain of approximately 8.57 dBi, and a maximum directivity of about 8.6 dB, as predicted by the computer simulation technology (CST) frequency-domain solver. These advantageous characteristics make the proposed antenna a suitable choice for point-to-point transmission applications.

Corresponding Author:

Mohammad Ahmed Alomari
Department of Engineering Technology
Faculty of Technology and Electronic and Computer Engineering (FTKEK)
Universiti Teknikal Malaysia Melaka (UTeM)
Melaka, Malaysia
Email: alomari@utem.edu.my

1. INTRODUCTION

The emergence of 5G technology marks a significant shift in global communication and interaction. However, as we consider this revolution in wireless communication, it is essential to acknowledge the pivotal role that the evolution of mobile communication has played in propelling modern technological advancements. From the era of bulky devices to the rise of smartphones and cellular networks, and now with the advent of 5G, mobile communications have profoundly shaped our technological landscape [1]–[4].

At the heart of this transformative journey lies the advancement of millimeter-wave technology. The millimeter-wave spectrum offers expanded bandwidth and accelerated data transfer rates compared to traditional microwave frequencies. The W-band (75–110 GHz), a subset of the millimeter-wave spectrum,

stands out for its short wavelengths and minimal atmospheric absorption loss, making it highly attractive for future developments. These frequency ranges hold immense potential for many wireless applications, including high-speed wireless communication networks, backhauling, precision radars, surveillance systems, high-resolution imaging, and biomedical applications. This breakthrough has not only revolutionized wireless communication but has also paved the way for cutting-edge applications like high-speed internet connectivity and immersive virtual and augmented reality experiences [5]–[9].

As the adoption of millimeter wave technology continues to grow, so does the importance of antenna design. Antennas serve as essential components in wireless systems, facilitating the transmission and reception of signals wirelessly. However, traditional antenna designs face limitations in effectiveness when operating at millimeter wave frequencies, necessitating the exploration of innovative solutions. One such solution gaining prominence is the patch antenna, offering potential avenues for overcoming these challenges [10], [11].

A growing body of research is focused on addressing the inherent limitations of microstrip antenna technology, especially in achieving desirable gain and bandwidth characteristics [12]–[22]. A notable study by [12] presents a single-band rectangular design to overcome these challenges. This design features square slots within the radiating patch, resulting in a resonant frequency of 73.7 GHz and a usable bandwidth ranging from 64.20 GHz to 77.45 GHz. The antenna is constructed using Rogers RT/Duroid 5880 material, with a precisely defined geometry of 5.8×7.3 mm² and material properties that support efficient wave propagation. These properties include a height of 0.55 mm, a loss tangent (tan δ) of 0.0009, and a permittivity (ε_r) of 2.2. Within its operational range, an impressive impedance bandwidth of 13.25 GHz is attained. This bandwidth is associated with an S_{11} value of -39.9 dB and a voltage standing wave ratio (VSWR) of 1.02.

Additionally, the design demonstrates a peak realized gain of 6.08 dB at the operation frequency. Another study introduces a multi-band rectangular patch antenna design featuring dual, geometric apertures etched into the radiating element [13]. This design exhibits seven distinct resonance frequencies ranging from 28.1 GHz to 82 GHz. The bandwidths associated with each resonance vary from 0.522 GHz (around 28.1 GHz) to 3.085 GHz (around 72.3 GHz). Additionally, the design demonstrates good return loss values across all operating bands. Notably, the antenna exhibits promising gain values, particularly at higher frequencies (reaching 7.168 dB at 60 GHz). The antenna is constructed using a Taconic TLY-3 substrate, which has dimensions of 12.5×12.5×0.508 mm³ and a permittivity of 2.2.

In Saeed et al. [14], a multi-band design targeting millimeter-wave applications for 5G is explained. This compact design with the size of 8.6×9.2×0.6 mm³ utilizes a cost-efficient Rogers RT/Duroid-5880 dielectric material. The antenna works at five distinct frequencies, ranging between 23.8 GHz to 93.9 GHz, and exhibits varying bandwidths across these bands, ranging from 1.47 GHz to 11.3 GHz. Additionally, the design achieves promising gain values, between 6.18 dBi and 7.7 dBi at the respective center frequencies. The work reported in [15] explains a miniaturized microstrip antenna designed to operate at a single frequency of 83 GHz. The antenna, measuring 2.02 mm×2.328 mm×0.149 mm, is installed on a Rogers RT/Duroid5880 material, which has a relative permittivity of 2.2. To achieve optimal impedance matching, the design incorporates an inset feed technique to ensure efficient signal transfer between the feed and the antenna. This antenna demonstrates a bandwidth of approximately 3.12 GHz, covering the frequencies from 81.3717 GHz to 84.4912 GHz. The design achieves an impressive return loss of over 55.79 dB, a VSWR of 1.0033, and a gain of 7.9087 dBi. Al-Khaffaf and Alshimaysawe [16] introduces a multi-band antenna design featuring a square-shaped radiating patch. The design utilizes the cost-effective FR-4 substrate with a relative permittivity of 3.9 and an overall size of 3.0714×3.0714×0.8 mm³, making it suitable for practical applications. The antenna operates across two distinct mm-wave bands. In the lower range extending from 43.5 GHz to 64 GHz, the antenna makes a gain of 3.49 dB, an S_{11} exceeding -42.42 dB, and a substantial bandwidth of 20.25 GHz. In addition, the antenna exhibits functionality in the higher frequency band ranging from 81 GHz to 95 GHz, within which it delivers a return loss exceeding 22.27 dB, a gain value of 4.52 dB, and a broad bandwidth of 14.09 GHz. Sateaa et al. [17] describe a design with a rectangular radiating patch operating at 60 and 93.7 GHz. This compact antenna measures 3.26 mm×3.94 mm with a height of 0.1 mm and is built on a Rogers RT5880 substrate having favorable electrical properties, including a dielectric constant of 2.2, and a low dielectric loss (tan δ) of 0.0009. At the resonance frequencies, it achieves bandwidths of 1.2 GHz and 1.1 GHz, indicating its ability to handle a range of signal variations. Furthermore, the design exhibits return losses exceeding 12 dB at both frequencies (14.34 dB at 60 GHz and 12.03 dB at 93.7 GHz). Additionally, the structure demonstrates acceptable impedance matching characteristics with VSWR of 1.475 and 1.6682 at the two operating frequencies. Finally, the design achieves promising gain values of 6.67 dBi and 6.88 dBi at the respective resonance frequencies.

Bhatia et al. [18] introduces a single-band antenna featuring dual semicircular slots in a rectangular configuration, tailored for 60 GHz operation. The design employs an inset feed technique to optimize signal transfer to the radiating patch. Built on Rogers RT/Duroid-5880 material with a dielectric constant of 2.2, the antenna has compact dimensions of 12×9.5×0.25 mm³, making it ideal for space-constrained applications. It achieves a maximum bandwidth of 1.75 GHz with a gain of 7.55 dBi. Adding a superstrate of specific height

enhances the bandwidth to 2.48 GHz and boosts the gain to 11.7 dBi. Moreover, a recent study [19] proposes a structure for the applications in the W and D bands. This structure uses an FR4 substrate with a dielectric constant of 4.3 and a loss tangent of 0.025. Measuring 4.8 mm×5.4 mm×1.6 mm³, the design exhibits multi-band functionality, operating at 35.84 GHz, 46.07 GHz, 56.74 GHz, 81.6 GHz, and 110.09 GHz. Notably, at the higher frequency bands, the antenna demonstrates impressive performance. It achieves a bandwidth of 3.3 GHz at 81.6 GHz and a wider bandwidth of 10.01 GHz at 110.09 GHz. Additionally, the design exhibits gain values of 6.22 dB and 8.51 dB, in addition to high radiation efficiencies exceeding 93.5%. Ali *et al.* [20] investigates an elliptical microstrip antenna designed for millimeter-wave applications in the V-band. The antenna is fabricated on a Rogers RT5880 substrate, with dimensions of 13×12×0.254 mm³, a dielectric constant of 2.2, and a loss tangent of 0.0009. It operates within the frequency range of 52.9 GHz to 70 GHz, delivering a realized gain that ranges from 7.97 dBi to 10.3 dBi across this spectrum. The research detailed in [21] introduces a novel tri-band antenna that operates at three distinct frequencies: 60 GHz, 94 GHz, and 110 GHz. At each of these frequencies, the antenna achieves good signal transmission efficiency, indicated by return loss values exceeding 11 dB. While impedance matching is satisfactory at 60 GHz and 110 GHz (VSWR below 1.2), the performance at 94 GHz shows a slight deviation (VSWR approaching 1.8). Despite this, the antenna maintains respectable gain values across the spectrum, ranging from 4.36 dB to 6.03 dB. Devana *et al.* [22] details a miniaturized, super wideband flower slotted microstrip patch antenna, designed for operation within the millimeter-wave spectrum extending from 3.78 to 109.86 GHz. This compact antenna, constructed using a FR-4 substrate, measures 16×22×1.6 mm³. Additionally, the antenna exhibits promising gain values across the spectrum, ranging from 4.23 dBi to 7.2 dBi, alongside radiation efficiencies that vary from 68.87% to 90.32%.

Building on the previous discussions, it is apparent that certain antenna designs struggle with issues like limited gain, narrow bandwidth, excessive size, or a combination of these problems. Consequently, this research aims to tackle these challenges by introducing a compact antenna that offers wide bandwidth and adequate gain. In this work, the authors propose an antenna tailored specifically for 5G communication applications, operating within the frequency band of 75 GHz to 110 GHz, commonly referred to as the W-band. This antenna is distinguished by its compact size and low profile, measuring 3.4×4×0.16 mm³. The antenna's performance was enhanced by incorporating two parasitic elements, adding a hexadecagon-shaped slot to the patch, and etching a ring slot on the ground plane. Significantly, the proposed structure fulfills a peak gain of 8.57 dBi. It also offers an impedance bandwidth of 28.54 GHz, corresponding to a fractional bandwidth of 30.38%, covering frequencies from 79.67 GHz to 108.21 GHz. Furthermore, the reflection coefficient of -59 dB demonstrates that the feed line is impressively matched to the patch. The design and optimization phases are conducted using the computer simulation technology (CST)-frequency domain solver (FD), followed by the validation of simulation results using the CST-time domain solver (TD).

The remaining parts of the manuscript are structured as follows. Section 2 elaborates on the design method and analysis utilized in the antenna construction, whereas section 3 investigates the effects of varying some antenna parameters on the reflection coefficient performance. Additionally, section 4 validates the simulation results and provides an array of simulation outcomes related to antenna attributes. Finally, section 5 concludes the study and identifies potential future research directions.

2. ANTENNA DESIGN METHOD

This section outlines the design process for the microstrip patch antenna proposed in this article. The design process begins with selecting the antenna shape and defining parameters such as operating frequency, required impedance bandwidth, targeted gain, and radiation efficiency. To achieve desirable antenna characteristics, we opted for a rectangular shape. Initially, we aim to design an antenna to resonate at 88 GHz and operate within the W-band spectrum from 75 GHz to 110 GHz. We chose the RT/Duroid 5880 dielectric material with a height (Hs) of 0.16 mm, a dielectric loss (tanδ) of 0.0009, and a relative permittivity (ε_r) of 2.2. To properly connect the feed line to the patch, we employed the inset feed technique to maximize return loss and ensure optimal matching. Once these initial design parameters were set, we calculated the remaining physical dimensions of the preliminary antenna using formulas detailed in the subsequent subsection. The design process unfolds in three stages, beginning with obtaining the basic design using mathematical models. The focus then shifts to enhancing the matching between the radiating patch and the feed line, followed by optimizing the antenna's performance.

2.1. Antenna mathematical model

In this section, we concisely overview the mathematical models employed to establish the initial dimensions of the rectangular microstrip patch antenna, as referenced in [23]–[25]. To begin with, we computed the dimensions of the radiating patch. The width (Wp) of the radiating element was derived using (1).

$$Wp = \frac{c}{2f_r}\sqrt{\frac{2}{\varepsilon_r+1}} \tag{1}$$

Here, ε_r represents the relative permittivity of the Rogers RT/Duroid 5880 dielectric substrate, and c denotes the speed of light. To determine the actual length of the patch (Lp), we initially compute the effective relative permittivity (ε_{reff}), followed by the calculation of the excessive length of the radiating element (ΔL) as demonstrated:

$$\varepsilon_{reff} = \frac{\varepsilon_r+1}{2} + \frac{\varepsilon_r-1}{2}\frac{1}{\sqrt{1+12\frac{Hs}{Wp}}} \tag{2}$$

where Hs is the substrate material height. ΔL, is then calculated using the:

$$\Delta L = 0.412 Hs \frac{(\varepsilon_{reff}+0.3)(\frac{Wp}{Hs}+0.264)}{(\varepsilon_{reff}-0.258)(\frac{Wp}{Hs}+0.8)} \tag{3}$$

Lp is therefore computed as (4).

$$Lp = \frac{c}{2f_r\sqrt{\varepsilon_{reff}}} - 2\Delta L \tag{4}$$

After establishing the initial dimensions of the radiating patch, we proceed to determine the width (Wg) and length (Lg) of the dielectric substrate material using the following equations. This step ensures that the substrate dimensions align appropriately with the radiating patch.

$$Wg = Wp + 6Hs \tag{5}$$

$$Lg = Lp + 6Hs \tag{6}$$

Afterward, we determine the feed line length (Lf) and width (Wf) using (7) through (9).

$$Lf = 3.96 \times Wf \tag{7}$$

$$Wf = \frac{2Hs}{\pi}\{B - 1 - ln(2B - 1) + \frac{\varepsilon_r-1}{2\varepsilon_r}[ln(B-1) + 0.39 - (\frac{0.61}{\varepsilon_r})]\} \tag{8}$$

$$B = \frac{377\pi}{2Z_o\sqrt{\varepsilon_r}} \tag{9}$$

The inset feed technique is employed to ensure proper impedance matching between the microstrip line and the patch element. The inset feed gap (Yo) can be calculated using:

$$Yo = \frac{4.65\times10^{-18}.c.f_r}{\sqrt{2\varepsilon_{reff}}} \tag{10}$$

where f_r is the operating frequency. Applying these models led to the initial antenna design depicted in Figure 1(a).

2.2. Antenna architecture
Figure 1 outlines the pivotal stages involved in refining the antenna design for optimization. Initially, as depicted in Figure 1(a), the initial design operates at 88 GHz, providing a bandwidth of 6.18 GHz and a return loss of 20.5 dB. In the subsequent phase shown in Figure 1(b), two parasitic elements were introduced to broaden the bandwidth, albeit resulting in a multi-band operation. However, this adjustment does not yield improvements in either the bandwidth or the return loss. Moving to the third phase, depicted in Figure 1(c), a ring slot was etched onto the ground plane. This alteration notably increased the impedance bandwidth to approximately 17 GHz and enhanced the gain to 8.42 dBi, while also improving the return loss. Transitioning to the fourth phase, a square slot with a length (Wo) of 0.126667 mm was added to the patch, followed by a second square slot of the same length rotated by 45 degrees, resulting in a hexadecagon-shaped slot as shown in Figure 1(d). This addition significantly enhanced the bandwidth to 28.54 GHz, accompanied by an impressive return loss of 59 dB, and a gain of 8.57 dB. Figure 2(a) shows the front view of the optimized antenna

configuration while Figure 2(b) depicts the back view with its key dimensions summarized in Table 1. Furthermore, the S_{11} performances across the various design phases are illustrated in Figure 3.

| (a) | (b) | (c) | (d) |
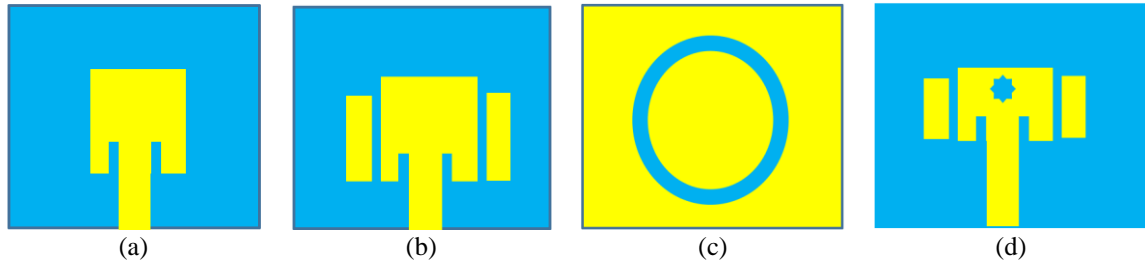
Figure 1. The stages of developing the antenna: (a) phase 1, (b) phase 2, (c) phase 3, and (d) phase 4

| (a) | (b) |
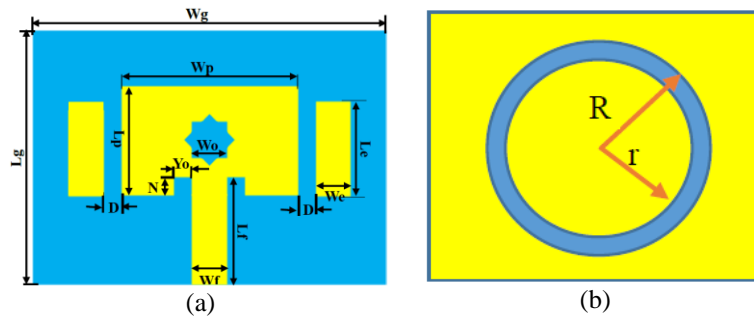
Figure 2. The optimized antenna: (a) front view and (b) back view

Table 1. Dimensions of the proposed antenna

Parameter	Symbol	Value (mm)	Parameter	Symbol	Value (mm)
Substrate width	Wg	4	Length of the inset gab	N	0.37
Substrate length	Lg	3.4	Hexadecagon length	Wo	0.126667
Substrate height	Hs	0.16	Outer radius of the ring slot	R	1.5
Width of the patch	Wp	1.354	Inner radius of the ring slot	r	1.25
Length of the patch	Lp	1.03	Distance between patch and parasitic element	D	0.1
Length of the feed line	Lf	1.19	Width of the parasitic element	We	0.4
Width of the feed line	Wf	0.08	Length of the parasitic element	Le	0.945
Width of the inset gab	Yo	0.06			
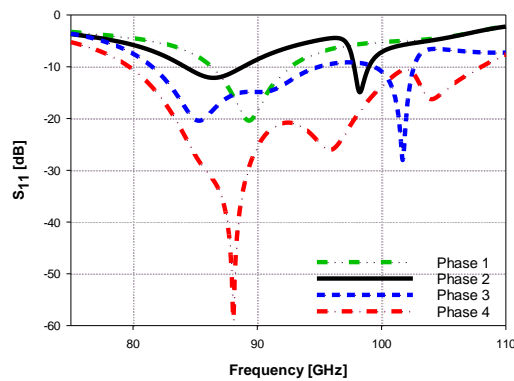
Figure 3. Simulated S_{11} performances of different design stages

3.   PARAMETRIC ANALYSIS

This section examines key parameters influencing the S_{11} performance of the proposed antenna. First, the impact of the separation distance (D) between the parasitic elements and the radiating patch is analyzed. Next, we investigate how varying the length (Le) and width (We) of the parasitic element affects performance.

Additionally, we assess the effect of modifying the dimension (Wo) of the hexadecagon slot polygon. Lastly, we explore the implications of adjusting the inner and outer radii of the ring slot. Conducting this parametric study is essential for optimizing the antenna design to achieve peak performance [26].

3.1. Effects of varying distance between the patch and its parasitic elements (D)

In this subsection, we explore how adjusting the distances between parasitic elements and the patch's edges (D) affects the S_{11} performance. Parameter D is varied from 0.08 mm to 0.14 mm in increments of 0.02 mm. The most favorable outcome, as shown by the red curve in Figure 4, occurs when D is 0.1 mm, yielding a maximum return loss of 59 dB. Interestingly, reducing D to 0.08 mm results in a drop in return loss to 44 dB, as indicated by the dotted black curve. Conversely, increasing D to 0.14 mm drops the return loss further to 40 dB, accompanied by a reduction in bandwidth.
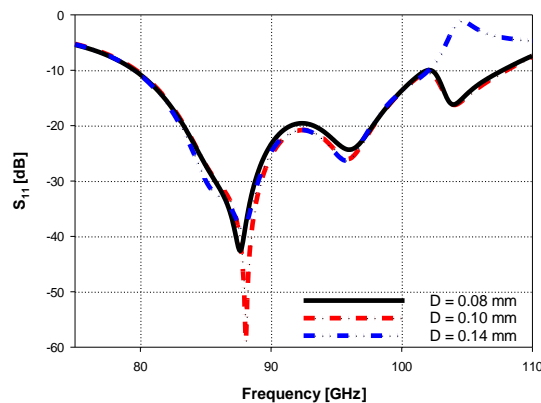
Figure 4. Effects of varying D on the S_{11} performance

3.2. Effects of varying Wo

Figure 5 illustrates the effect of varying the value of the parameter, Wo, on the S_{11} performance. Figure 5 shows that the optimal value of Wo is 0.126667 mm, at which the optimal performance is achieved, with a bandwidth of approximately 28.54 GHz and a return loss of 59 dB. When the value of Wo is increased to 0.14 mm, the return loss decreases to 40 dB and the bandwidth decreases as well, as shown by the blue curve. Similarly, when the value is decreased to 0.1 mm, the return loss decreases, as shown by the black curve. Figure 5 also shows that the resonance frequency does not change.
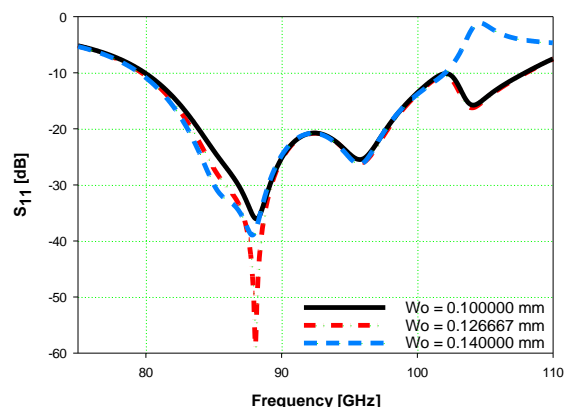
Figure 5. Effects of varying the value of Wo on S_{11} performance

3.3. Effects of varying the ring's radii

This subsection investigates the effects of altering the outer (R) and inner (r) radii of the ring slot on the S_{11} performance. Figure 6 shows the impacts of varying the value of the outer radius of the ring (R) on S_{11} performance. The red curve represents the optimal performance when the value of R is set to 1.5 mm, achieving

a bandwidth of approximately 28.54 GHz and a return loss of up to 59 dB. When the value of R reduces to 1.4 mm, the return loss decreases to 15 dB, with a noticeable reduction in the impedance bandwidth, as shown by the blue curve. Similarly, when R increases to 1.7 mm, the center frequency shifts up to approximately 96 GHz with a reduction in the return loss to 30 dB, as shown by the black curve. Figure 7 plots the S_{11} performances for different values of the parameter (r). As shown, the optimal value for this parameter is 1.25 mm, at which the S_{11} performance is the optimum. Changing its value leads to a reduction in the impedance bandwidth, lowering the return loss value, and shifting the resonance frequency.
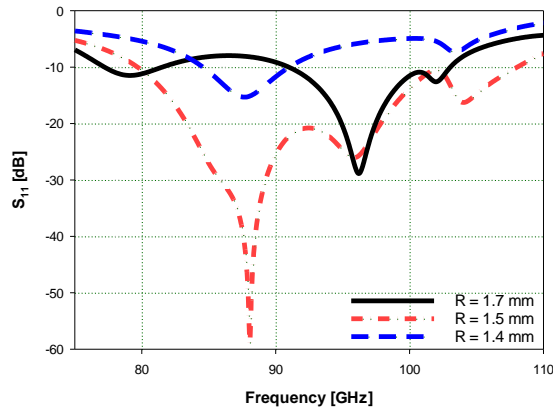
Figure 6. Effects of varying the value of R on S_{11} performance
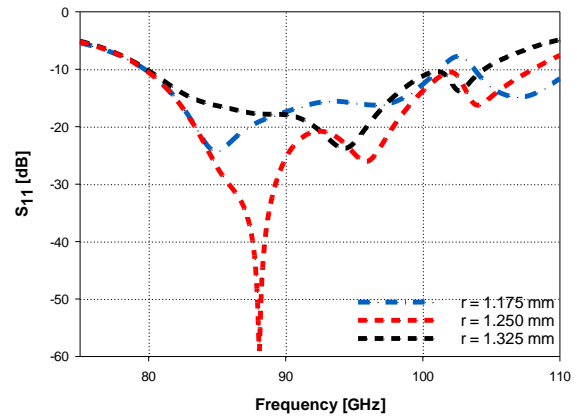
Figure 7. Effects of varying the value of r on S_{11} performance

3.4. Effects of varying parasitic elements' dimensions (Le and We)

The desired performance is illustrated by the red curve in Figure 8, where the length of the parasitic elements is optimized at 0.945 mm. This design achieves the best return loss of 59 dB with a bandwidth of 28.54 GHz. When the length of the parasitic components is reduced to 0.795 mm, the resonance frequency shifts to 89.5 GHz, the bandwidth narrows slightly, and the return loss decreases to 32 dB. Additionally, as depicted by the blue curve, increasing the parasitic length to 1.045 mm results in the resonance frequency shifting to 98.5 GHz, the bandwidth reducing to 11.47 GHz, while the return loss remains unchanged.
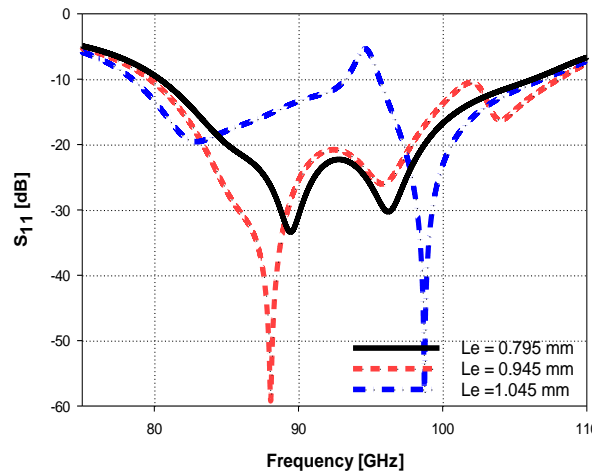
Figure 8. Effects of varying the value of Le on S_{11} performance

On contrary, changing the value of the parasitic element's width (We) has no impact on the bandwidth of the antenna. However, increasing or decreasing the value of this parameter will affect the S_{11} value and shift the resonance frequency down as shown in Figure 9.
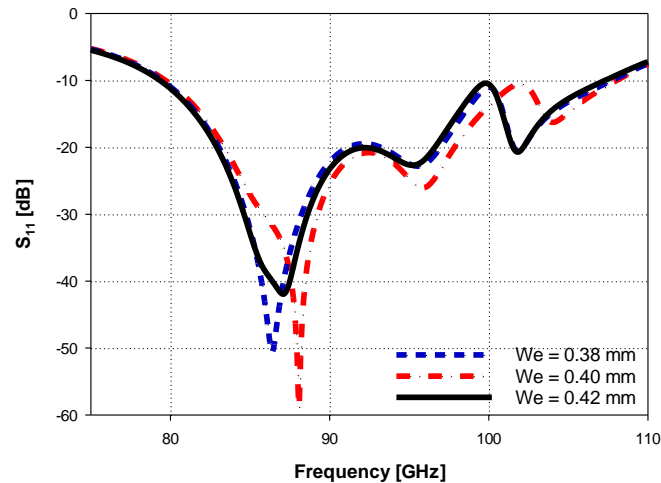
Figure 9. Effects of varying the value of We on S_{11} performance

4. SIMULATION RESULTS AND DISCUSSION

This section thoroughly analyzes several key aspects of the antenna's performance, encompassing the S_{11}, VSWR, 2D, and 3D radiation characteristics, surface current distribution, gain, directivity, and radiation efficiency. The optimization of the antenna's performance is evaluated through comprehensive simulations conducted using CST, employing both frequency (FD) and time (TD) solvers. While the FD was primarily utilized for design and optimization, validation of outcomes was ensured through examination with the TD. This integrated approach allows for a comprehensive assessment of the antenna's behavior across different domains, ensuring robustness and accuracy in the evaluation process.

4.1. The reflection coefficient (S_{11})

Figure 10 depicts the S_{11} curves for the optimized antenna, generated by the frequency and TD. Both solvers predict the same impedance bandwidth. The return loss obtained from the FD is substantially better than that from the TD ($S_{11}\approx$-59 dB as expected by the frequency solver). Furthermore, the resonance occurs at 88 GHz, as attained by the frequency solver, although the resonance frequency predicted by the time solver is also somewhat lower than 88 GHz (at $f_r \approx$86 GHz). Nonetheless, there is a considerable agreement between the S_{11} performance expected by frequency and time solvers. Figure 10 indicates that the suggested antenna resonates at exactly 88 GHz with a return loss of 59 dB and an impedance bandwidth ($\leq$-10 dB) of 28.54 GHz (79.67 GHz-108.21 GHz) when considering the FD.
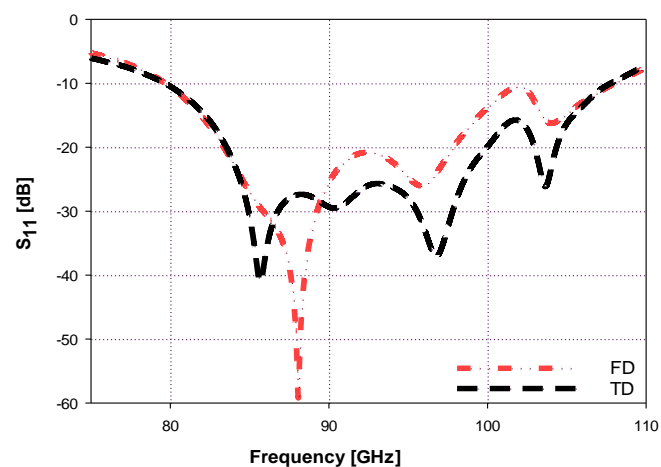
Figure 10. Simulated S_{11} performance of the proposed antenna using frequency and time solvers

4.2. Voltage standing wave ratio

Figure 11 illustrates the VSWR performance of the proposed antenna. Across the operational band, both the frequency and time solvers predict the same bandwidth for VSWR≤2. It is noticeable that the VSWR value at resonance is 1.002. The fact that VSWR remains ≤2 throughout the operating band suggests effective matching between the feed line and the radiating patch [27]–[29].
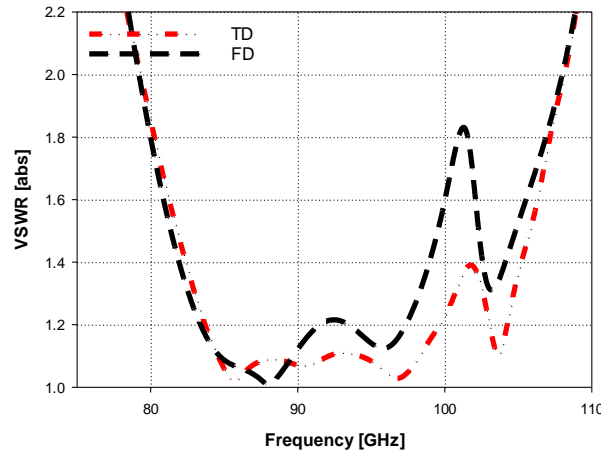
Figure 11. Simulated VSWR of the proposed antenna using frequency and time solvers

4.3. Radiation characteristics

Antenna gain, a crucial performance metric, reflects its effectiveness in transmitting and receiving signals in a particular direction. It is influenced by two main factors: antenna directivity and radiation efficiency. The 3D radiation patterns generated by both the frequency and time solvers for the proposed design at the resonance frequency are illustrated in Figures 12(a) and (b). These patterns highlight the directional nature of the antenna radiation, with the frequency-solver predicting a gain of 8.404 dBi, while the time-solver forecasts an almost equal gain of 8.408 dBi at the resonant frequency. However, the maximum gain predicted by the FD is 8.57 dBi.
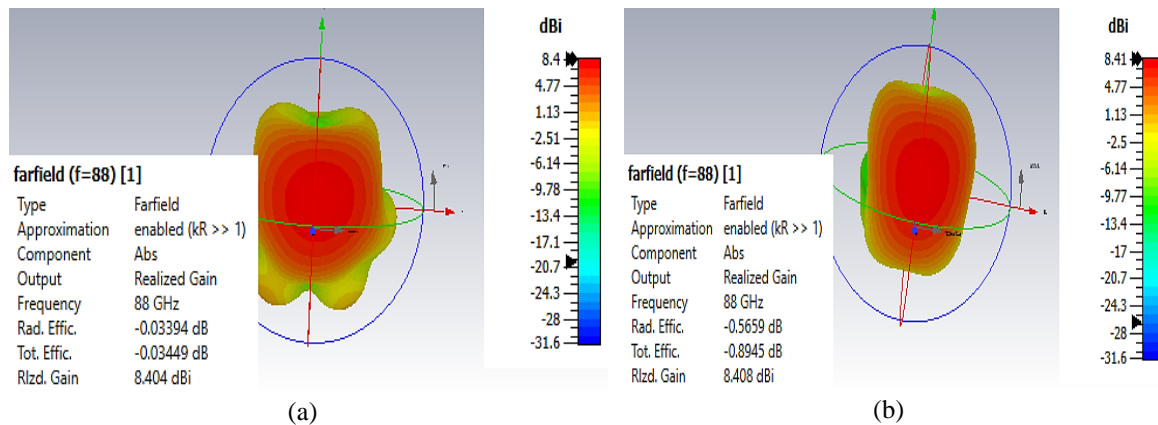
Figure 12. The 3D radiation pattern at 88 GHz: (a) FD and (b) TD

Additionally, Figures 13(a) and (b) illustrates the 2D radiation patterns in both the E (phi=0º) and H (phi=90º) planes at the resonance frequency, of 88 GHz. A close comparison between the simulated radiation patterns from the frequency and time solvers reveals a good agreement. These 2D patterns highlight effective antenna directionality, with peak radiation concentrated in the boresight direction of the radiating patch.

(a)   (b)
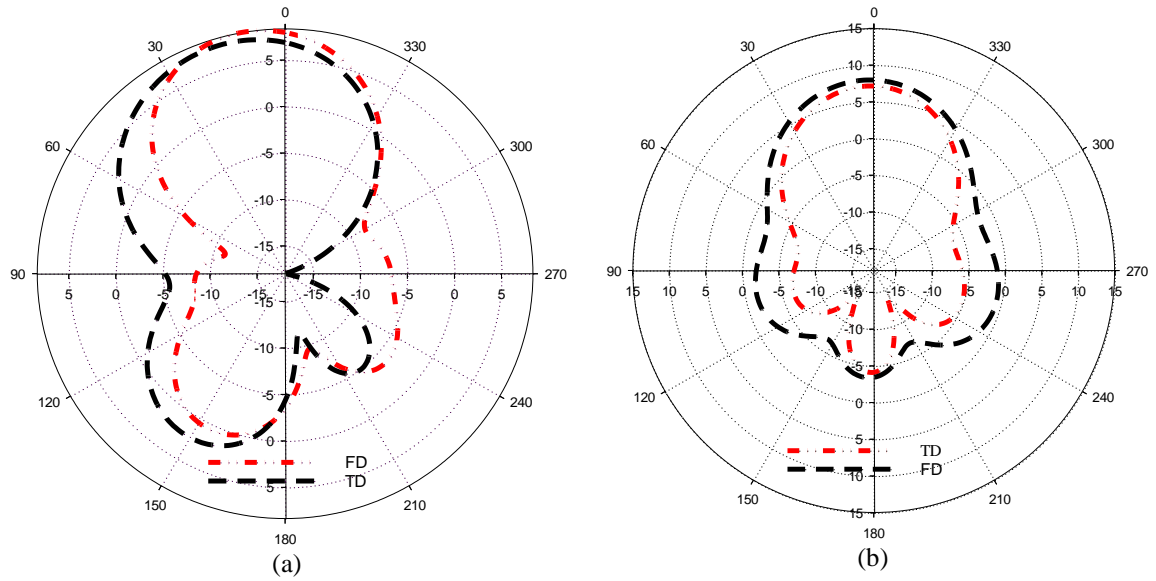
Figure 13. 2D radiation patterns at 88 GHz: (a) phi=0º and (b) phi=90º

Figure 14 demonstrates the variations in gain, and directivity across the operating band using the CST (time-domain solver). Notably, the antenna achieves a peak gain slightly over 9 dBi at 83.7 GHz and a minimum gain of 4.9 dBi at 95.3 GHz, with a gain of 8.4 dBi at the resonant frequency. Similarly, the directivity ranges from 5.9 dBi at 93 GHz to 9.6 dBi at 86 GHz, with a directivity of 9.2 dB at resonance.

4.4. Surface current distribution

The surface current distribution at 88 GHz is depicted in Figure 15. Current concentration is observed along the feed line, at the edges of the inset feed gap, and around the edges of the hexadecagonal-shaped slot. Notably, the current density around the outer edges of the inset measures 151 A/m.
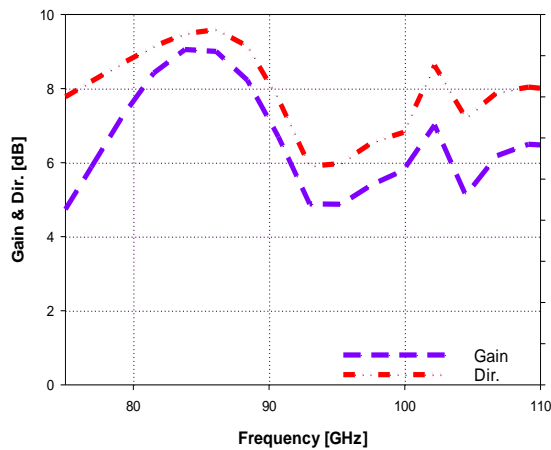
Figure 14. Gain and directivity vs frequency (TD)
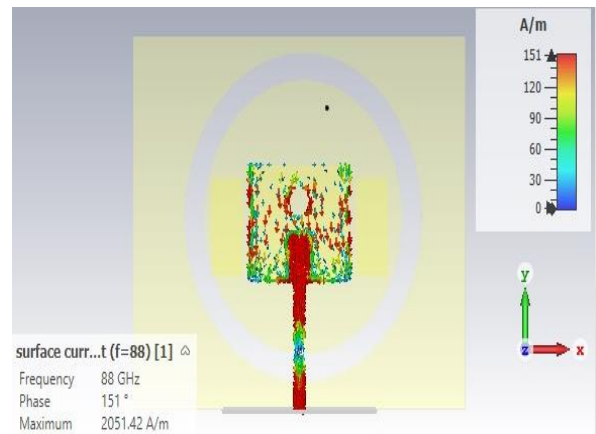
Figure 15. Surface current distribution at 88 GHz

4.5. Comparison with some recently published works

Table 2 provides a summary of the performance results of the proposed design and a comparative analysis between our proposed antenna and several designs from the literature, focusing on parameters such as antenna dimensions, operating bandwidth, radiation efficiency, reflection coefficient, and peak gain. The proposed antenna outperforms the designs in [12], [13], [15]–[17], [19] in terms of gain, reflection coefficient, and VSWR. Additionally, it operates over a broader bandwidth than the antennas described in [12], [13], [15],

[17], [19]. In terms of size, the proposed antenna is more compact than those in [12], [13]. Furthermore, its radiation efficiency surpasses that of the antenna in [13] and is comparable to the one in [19].

Table 2. Summary of the results and comparison with some designs from the published literature

Ref.	[12]	[13]	[15]	[16]	[17]	[19]	This work
f_r (GHz)	73.7	28.1/36.7/45.8/55.2/62.8/72.3/82	83	60/90	60/93.7	81.6/110	88
Size (mm³)	5.8×7.3×0.55	12.5×12.5×0.508	2.02×2.328×0.149	3.0714×3.0714×0.8	3.26×3.94×0.1	4.8×5.4×1.6	3.4×4×0.16
BW (GHz)	13.25	12.36 (total)	3.12	20.25/14.09	1.2/1.1	4.04/9.09	28.54
Gain (dBi)	6.08	≤7.168	7.9	3.49/4.52	6.67/6.88	6.22/8.5	8.57
S_{11} (dB)	- 39.9	−35.203/−41.149/−18.787/−12.196/−16.002/−15.148	-55.8	-42.42/-22.27	-14.34/-12.03	-24.4/-15.9	-59
VSWR	1.02	-	1.003	-	1.48/ 1.67	1.13/1.38	1.002
Rad. Eff. (%)	-	86 (max)	-	-	-	94.06 (max)	91.5

5. CONCLUSION

This study proposes a slotted antenna with two parasitic elements for W-band applications. The design features a simple rectangular structure fed by a microstrip line with an inset feed. To enhance performance, two rectangular parasitic elements were placed near the radiating patch. Additionally, a ring slot was etched on the ground plane, and a hexadecagon-shaped slot was introduced into the radiating patch to improve gain and bandwidth. Operating at 88 GHz, the antenna covers a bandwidth ranging from 79.67 GHz to 108.21 GHz. Built on a Rogers RT/Duroid 5880 substrate with a relative permittivity of 2.2 and a loss tangent of 0.0009, the antenna has compact dimensions of 3.4×4×0.16 mm³. The suggested structure achieves a fractional bandwidth of 30.38% (S11<-10 dB), with a peak gain of 8.57 dBi and a directivity of 8.6 dB. These characteristics make the antenna suitable for high-speed transmission, advanced millimeter-wave systems, and applications such as wireless communication and radar. Future research will focus on developing a multiple-input multiple-output (MIMO) antenna based on this element to further improve transmission rates and enhance radiation gain.

REFERENCES

[1] J. G. Andrews, S. Buzzi, W. Choi, S. V. Hanly, A. Lozano, A. C. K. Soong, and J. C. Zhang, "What will 5G be?" *IEEE Journal on Selected Areas in Communications*, vol. 32, no. 6, pp. 1065-1082, 2014, doi: 10.1109/JSAC.2014.2328098.

[2] V. Sharma, N. K. Mishra, A. Agarwal, and N. L. Gupta, "Small size broadband printed antenna for 5G applications covering 28 GHz/38 GHz and 60 GHz bands," *Gazi University Journal of Science*, vol. 37, no. 1, pp. 211-220, 2024, doi: 10.35378/gujs.1178594.

[3] B. Bertenyi, "5G evolution: What's next?," *IEEE Wireless Communications*, vol. 28, no. 1, pp. 4-8, 2021, doi: 10.1109/MWC.2021.9363048.

[4] S. Irıqat and S. Yenikaya, "Microstrip patch antenna design with enhanced radiation efficiency for 5G 60 GHz millimeter-wave systems," *Uludağ Üniversitesi Mühendislik Fakültesi Dergisi.*, vol. 29, no. 1, pp. 101-112, 2024, doi: 10.17482/uumfd.1366173.

[5] S. Agarwal, N. P. Pathak, and D. Singh, "Concurrent 83GHz/94 GHz parasitically coupled defected microstrip feedline antenna for millimeter wave applications," in *2013 IEEE Applied Electromagnetics Conference (AEMC)*, Bhubaneswar, India, 2013, pp. 1-2, doi: 10.1109/AEMC.2013.7045120.

[6] G. Chittimoju and U. D. Yalavarthi, "A comprehensive review on millimeter waves applications and antennas," *Journal of Physics: Conference Series*, vol. 1804, no. 1, pp. 1-8, 2021, doi: 10.1088/1742-6596/1804/1/012205.

[7] M. A. Khattak, M. I. Khattak, S. M. Owais, A. A. Khattak, and A. Sultan, "Design and analysis of millimeter wave dielectric resonator antenna for 5G wireless communication systems," *Progress In Electromagnetics Research C*, vol. 98, pp. 239-255, 2020, doi: 10.2528/PIERC19102404.

[8] J. Doo, W. Park, W. Choe, and J. Jeong, "Design of broadband W-Band waveguide package and application to low noise amplifier module," *Electronics*, vol. 8, no. 5, pp. 1-9, 2019, doi: 10.3390/electronics8050523.

[9] Y. Zhang, A. R. Vilenskiy, and M. V. Ivashina, "W-band waveguide antenna elements for wideband and wide-scan array antenna applications for beyond 5G," in *2021 15th European Conference on Antennas and Propagation (EuCAP)*, 2021, pp. 1-5, doi: 10.23919/EuCAP51087.2021.9411184.

[10] D. Imran, M. M. Farooqi, M. I. Khattak, Z. Ullah, M. I. Khan, M. A. Khattak, and H. Dar, "Millimeter wave microstrip patch antenna for 5G mobile communication," in *2018 International Conference on Engineering and Emerging Technologies (ICEET)*, pp. 1-6, 2018, doi: 10.1109/ICEET1.2018.8338623.

[11] S. P. Rajan and C. Vivek, "Analysis and design of microstrip patch antenna for radar communication," *Journal of Electrical Engineering & Technology*, vol. 14, pp. 923-929, 2019, doi: 10.1007/s42835-018-00072-y.

[12] A. M. H. Aoun, A. A. Saeed, A. S. A. Gaid, O. Y. A. Saeed, M. N. G. Mohammed, and B. Hawash, "E-band slotted microstrip patch antenna for 5G mobile backhaul applications," in *2021 International Conference of Technology, Science and Administration (ICTSA)*, pp. 1-5, 2021, doi: 10.1109/ICTSA52017.2021.9406550.

[13] W. Shahjehan, I. Hussain, K. Amin, I. Ali, A. Riaz, and P. Uthansakul, "Hepta-band antenna for 5G applications," *Wireless Personal Communications*, vol. 125, no. 3, pp. 2031-2054, 2022, doi:10.1007/s11277-022-09644-8.

[14] A. A. Aoun, O. Y. A. Saeed, A. S. A. Gaid, A. M. H. Aoun, and A. A. Sallam, "A low profile multiband microstrip patch antenna for 5G mm-wave wireless applications," in *2021 International Conference of Technology, Science and Administration (ICTSA)*, pp. 1-5, IEEE, 2021, doi: 10.1109/ICTSA52017.2021.9406519.

[15] A. S. A. Gaid, S. M. E. Saleh, A. H. M. Qahtan, S. G. Aqlan, B. A. E. Yousef, and A. A. Saeed, "83 GHz Microstrip Patch Antenna for Millimeter Wave Applications," in *2021 International Conference of Technology, Science and Administration (ICTSA)*, pp. 1-4, IEEE, 2021, doi: 10.1109/ICTSA52017.2021.9406546.

[16] D. A. J. Al-Khaffaf and I. A. Alshimaysawe, "Miniaturised tri-band microstrip patch antenna design for radio and millimetre waves of 5G devices," *Indonesian Journal of Electrical Engineering and Computer Science*, vol. 21, no. 3, pp. 1594-1601, 2021, doi: 10.11591/ijeecs.v21.i3.pp1594-1601.

[17] S. D. Sateaa, M. S. Hussein, Z. G. Faisal, A. M. Abood, and H. D. Satea, "Design and simulation of dual-band rectangular microstrip patch array antenna for millimeter-wave," *Bulletin of Electrical Engineering and Informatics*, vol. 11, no. 1, pp. 299-309, 2022, doi: 10.11591/eei.v11i1.3336.

[18] S. Bhatia, D. Pal, and A. K. Bandyopadhyay, "Design and characterization of high gain semicircular slotted V-band printed antenna/array with superstrate," in *2023 3rd International Conference on Range Technology (ICORT)*, IEEE, 2023, pp. 1-4, doi: 10.1109/ICORT56052.2023.10249143.

[19] A. K. Galib, N. Sarker, and M. R. H. Mondal, "Novel multiband millimeter wave antennas," *Journal of Communications*, vol. 18, no. 1, pp. 1-14, 2023, doi: 10.12720/jcm.18.1.1-14.

[20] W. A. Ali, M. A. Abdelghany, and A. A. Ibrahim, "Wideband and high gain elliptically-inspired 4×4 MIMO antenna for millimeter wave applications," *Heliyon*, 2024, doi: 10.1016/j.heliyon.2024.e38697.

[21] A. Ahmed, H. M. A. Rahman, and M. M. Khan, "Design and analysis of a compact wideband V-band and W-band antenna for healthcare applications," in *2022 IEEE 12th Annual Computing and Communication Workshop and Conference (CCWC)*, pp. 1043-1048, 2022, doi: 10.1109/CCWC54503.2022.9720767.

[22] V. N. K. R. Devana, A. Beno, M. S. Alzaidi, P. B. M. Krishna, G. Divyamrutha, W. A. Awan, T. A. Alghamdi, and M. Alathbah, "A high bandwidth dimension ratio compact super wide band-flower slotted microstrip patch antenna for millimeter wireless applications," *Heliyon*, vol. 10, no. 1, 2024, doi: 10.1016/j.heliyon.2023.e23712.

[23] S. A. Ayoob, F. S. Alsharbaty, and A. N. Hammodat, "Design and simulation of high-efficiency rectangular microstrip patch antenna using artificial intelligence for the 6G era," *TELKOMNIKA (Telecommunication Computing Electronics and Control)*, vol. 21, no. 6, pp. 1234–1245, 2023, doi: 10.12928/TELKOMNIKA.v21i6.25389.

[24] R. Przesmycki, M. Bugaj, and L. Nowosielski, "Broadband microstrip antenna for 5G wireless systems operating at 28 GHz," *Electronics*, vol. 10, no. 1, pp. 1, 2020, doi:10.3390/ electronics10010001.

[25] A. S. A. Gaid, M. A. M. Ali, A. Saif, and W. A. A. Mohammed, "Design and analysis of a low profile, high gain rectangular microstrip patch antenna for 28 GHz applications," *Cogent Engineering*, vol. 11, no. 1, Art. no. 2322827, 2024, doi:10.1080/23311916.2024.2322827.

[26] R. R. Elsharkawy, "A compact super-wideband MIMO antenna for wireless communication systems," *Progress in Electromagnetics Research M*, vol. 129, pp. 119–129, 2024, doi: doi:10.2528/PIERM24082006.

[27] F. ALtalqi, S. Fennane, H. Mabchour, H. Kacimi, and A. Echchelh, "Design monopole antenna of ultra-wideband high bandwidth and high efficiency for ground penetrating radar application," *TELKOMNIKA (Telecommunication Computing Electronics and Control)*, vol. 22, no. 4, pp. 812-821, 2024, doi: 10.12928/TELKOMNIKA.v22i4.25340.

[28] A. S. A. Gaid, N. S. Ala'a, and M. A. Alomari, "A compact microstrip antenna with dual thin slits for high-capacity data streaming in the 38 and 39 GHz bands for 5G applications," *Results in Engineering*, vol. 24, 2024, doi: 10.1016/j.rineng.2024.103411.

[29] F. ALtalqi, H. Mabchour, and A. Echchelh, "Design of a high-efficiency monopole antenna array for GPR application," *Journal of Nano-and Electronic Physics,* vol. 16, no. 2, 2023, doi: 10.21272/jnep.16(2).02015.

BIOGRAPHIES OF AUTHORS

AbdulGuddoos S. A. Gaid obtained a B.Eng. in electronics engineering from the Sudan University for Science and Technology (SUST), Khartoum, Sudan, in 2000. He pursued an M.Eng. and a Ph.D. in electrical, electronic, and systems engineering from Universiti Kebangsaan Malaysia (UKM) in 2004 and 2010, respectively. After joining Taylor's University in September 2010, he served as a lecturer until August 2012. From September 2012 onward. He has been a faculty member at the Department of Communication and Computer, Faculty of Engineering, Taiz University. He teaches various courses in electrical, electronics, and communications. His primary research areas include wireless communications and microstrip patch antennas for wireless communication networks. He has a publication record of over 35 conference and journal papers and has actively contributed to organizing committees for conferences such as the International Conference on Technology, Science, and Administration (ICTSA 2021) and the 3rd International Conference on Emerging Smart Technologies and Applications (eSmarTA 2023) held at Taiz University. He can be contacted at email: quddoos.gaid@taiz.edu.ye.

Mohammed M. S. Qaid 🆔 🔍 SC 🔗 received his Bachelor's degree in communication and computer engineering from the Faculty of Engineering and Information Technology, Taiz University, Yemen in the year 2024. He has a strong interest in the advancement of wireless communication systems, particularly in the optimization of heterogeneous network environments. He aspires to further his academic career at a prestigious institution to refine his research skills and contribute to the development of innovative telecommunications solutions. He can be contacted at email: mohammedalwhapi2@gmail.com.

Mohammed A. E. Abdullah 🆔 🔍 SC 🔗 earned his Bachelor's degree in communication and computer engineering from the Faculty of Engineering and Information Technology at Taiz University, Yemen, in 2024. His research interests include heterogeneous networks and microstrip antennas for 5G wireless communications. He aims to pursue advanced studies at a renowned institution to enhance his research expertise and contribute to the advancement of innovative solutions in telecommunications. He can be contacted at email: mohammed.abdullah.std@taiz.edu.ye.

Mohammad Ahmed Alomari 🆔 🔍 SC 🔗 is affiliated to the Faculty of Technology and Electronic and Computer Engineering (FTKEK), Universiti Teknikal Malaysia Melaka (UTeM), Melaka, Malaysia, where he is currently working as a senior lecturer. He received his M.Sc. and Ph.D. in computer systems engineering from Universiti Putra Malaysia (UPM), Malaysia. This author became a member (M) of IEEE in 2010, and a Senior Member (SM) in 2020. His major research interests include data storage encryption in mobiles, security of smart renewable energy and smart grid, embedded systems, and cryptography. He is currently extending his research to the internet of things (IoT), blockchain technology, and cloud computing. He has authored and co-authored several national and international publications in journals and international conferences, while he is working as a reviewer for worldwide reputable journals in Springer and SAI organization. He is a member of organizing and technical committees of many international conferences and workshops in Malaysia and Japan. He is also a member of the International Association of Engineers (IAENG), and the Malaysian Society for Engineering and Technology (MySET). He can be contacted at email: alomari@utem.edu.my.